Adaptive Second-Order Sliding-Mode Observer for PMSM Sensorless Control Considering VSI Nonlinearity

Donglai Liang, *Student Member, IEEE*, Jian Li, *Member, IEEE*, Ronghai Qu, *Fellow, IEEE*, and Wubin Kong, *Member, IEEE*

***Abstract*—This paper proposes an adaptive super-twisting algorithm based sliding-mode observer (STA-SMO) for surface-mounted permanent magnet synchronous machine (PMSM) sensorless control, in which voltage source inverter (VSI) nonlinearity is taken into consideration. An adaptive algorithm for online tuning the sliding-mode coefficients of STA-SMO is proposed based on the existing stable conditions. Thus, position estimation error can be reduced by the proposed adaptive algorithm in wide-speed range. Furthermore, voltage distortion due to VSI nonlinearity is online compensated to improve the accuracy of PMSM model. Because mismatch between reference and actual voltage due to VSI nonlinearity may bring large rotor position and speed estimation error, especially in low-speed range where distorted voltages may become dominant compared to actual voltages. Thus, a STA-SMO with adaptive sliding-mode coefficients and accurate voltage value could be obtained. Finally, the effectiveness of the proposed adaptive STA-SMO with online VSI nonlinearity compensation is verified on a surface-mounted PMSM by experiments.**

***Index Terms*—Adaptive super-twisting algorithm (STA), permanent magnet synchronous machine (PMSM), sensorless control, sliding-mode observer, voltage-source inverter (VSI) nonlinearity compensation.**

I. Introduction

In THE last decade, permanent magnet synchronous machine (PMSM) has been widely used in industry area. In order to enhance the reliability and reduce the cost, position sensorless control has gained extensive attention since the 1980s [1]. There are two main categories of sensorless control techniques for PMSM, including high frequency injection methods based on saliency tracking [2]–[4] and back ElectroMotive Force (back-EMF) methods based on machine model [5]–[13].

Although high frequency injection methods works well in zero and low speed range, its application to nonsalient surface-mounted PMSM sensorless control is difficult [14]. Besides, injected high frequency signals may cause fluctuations in q-axis current and torque ripple. On the contrary, machine model based sensorless control methods, including model reference adaptive system (MRAS) [5], extended Kalman filter (EKF) [6] and sliding-mode observer (SMO) [7]–[10], are suitable for medium and high speed range sensorless operation where back-EMF is large enough to be estimated. For machine model based sensorless techniques, MRAS may have a difficulty in the model parameters adaptation. For example, motor parameters are identified online to improve the performance of MRAS based sensorless control [5]. EKF based sensorless techniques work well in noisy environment. However, high-performance digital signal processor (DSP) or field programmable gate array are necessary for heavy online matrix computing [6].

SMO based methods are recognized for their robustness against parameter variation and simplicity. However, traditional SMO is bothered by chattering problem. And hence, low-pass filter (LPF) and phase compensation are necessary, which will increase the complexity of the system. In order to reduce chattering problem and simplify the control system, various second-order SMOs, such as twisting algorithm and super-twisting algorithm (STA), have been proposed [15]. Super-twisting algorithm is widely employed in observers and controllers due to its chattering-free characteristic [7]–[9], [16]–[19]. In [7], [16]–[18], STA based SMO (STA-SMO) is employed for sensorless control of induction machine or PMSM to reduce chattering problem and estimation error. However, constant sliding-mode coefficients are adopted in these methods, which means high-performance sensorless operation is restricted in limited speed range. That is because the existing stable conditions for STA-SMO are vague and it is difficult to adjust the sliding-mode coefficients online to maintain good performance at different speed. In other words, the robustness against disturbances of STA-SMO with constant sliding-mode coefficients is weak. One effective solution is to use adaptive observers. Many researchers have proposed various adaptive algorithms to improve the performance of controllers and observers [20]–[28]. In [20], an adaptive interconnected observer is proposed for PMSM sensorless control and shows strong robustness against parameters variation. In [26], two types of adaptive observers, including adaptive sliding-mode observer and backstepping observer, are proposed to improve the estimation accuracy of rotor speed. Similarly, an adaptive algorithm is also proposed in this paper

Manuscript received August 15, 2017; revised November 14, 2017; accepted December 11, 2017. Date of publication December 15, 2017; date of current version July 15, 2018. Recommended for publication by Associate Editor J. Olorunfemi. *(Corresponding author: Jian Li.)*

The authors are with the State Key Laboratory of Advanced Electromagnetic Engineering and Technology, School of Electrical and Electronic Engineering, Huazhong University of Science and Technology, Wuhan 430074, China (e-mail: liangdonglai@hust.edu.cn; jianli@hust.edu.cn; ronghaiqu@mail.hust.edu.cn; wubinkong@126.com).

Color versions of one or more of the figures in this paper are available online at http://ieeexplore.ieee.org.

Digital Object Identifier 10.1109/TPEL.2017.2783920

to improve the estimation accuracy in wide-speed range and the details of the proposed adaptive algorithm will be introduced later.

In practice, the performance of model based sensorless techniques is poor in low speed due to low back-EMF, voltage source inverter (VSI) nonlinearity, etc. Estimation error caused by low back-EMF can be reduced by employing high-precision but expensive current sensors. VSI nonlinearity is caused by dead-time, turn-on/off delay and voltage drop across switches, which cannot be eliminated. This nonlinearity will cause voltage distortion, resulting in mismatch between reference and actual voltage [29]. Generally, reference voltages instead of measured voltages are used for position estimation. Therefore, distorted reference voltages will bring position estimation error and, hence, VSI nonlinearity should be compensated. VSI nonlinearity compensation techniques have been widely reported in [29]–[35]. However, accurate machine parameters are necessary for VSI nonlinearity compensation in these methods [29]–[33]. In order to improve the robustness of the VSI nonlinearity compensation method, a machine parameter-independent technique is proposed in this paper.

In this paper, an adaptive STA-SMO considering VSI nonlinearity for PMSM sensorless control is proposed. A STA-SMO is used to estimate the back-EMFs for position sensorless control. At the same time, an adaptive algorithm is proposed for online tuning the sliding-mode coefficients, which can reduce the position estimation error in wide-speed range and simplify the use of STA-SMO on PMSM sensorless control. The stability analysis is proved based on the existing stable conditions. Furthermore, a machine parameter-independent, simple and effective VSI nonlinearity compensation technique is proposed to reduce the distorted voltages caused by VSI nonlinearity. The proposed VSI nonlinearity compensation method is suitable for $i_d = 0$ control, which is widely employed in surface-mounted PMSM. Distorted voltages are obtained without using machine parameters and VSI nonlinearity is online compensated by minimizing the distorted voltages. Thus, a more accurate PMSM model for position estimation can be obtained. Finally, the effectiveness of the proposed adaptive STA-SMO with VSI nonlinearity compensation is validated by experiments.

II. Adaptive STA-SMO

The mathematic model of surface-mounted PMSM can be written as state equation form in the $\alpha\beta$ stationary reference frame as [9]

$$\frac{di_\alpha}{dt} = -\frac{R}{L}i_\alpha + \frac{1}{L}u_\alpha - \frac{1}{L}e_\alpha \tag{1a}$$

$$\frac{di_\beta}{dt} = -\frac{R}{L}i_\beta + \frac{1}{L}u_\beta - \frac{1}{L}e_\beta \tag{1b}$$

where $i_{\alpha\beta}$, R, L, $u_{\alpha\beta}$, and $e_{\alpha\beta}$ are $\alpha\beta$-axis currents, stator resistance, stator inductance, $\alpha\beta$-axis voltages, and $\alpha\beta$-axis back-EMFs, respectively. It should be noticed that the surface-mounted PMSM used in this paper is assumed to be symmetric and the magnet motive force harmonics are ignored. Since variables used in (1) do not depend on rotor position, $\alpha\beta$-axis voltage equations is a good choice for model based sensorless control method.

A. Super-Twisting Algorithm

STA is proposed by Levant in [36] for controller and observer design [37], [38]. The basic form of STA is presented as

$$\begin{aligned}\frac{dx_1}{dt} &= -k_1|\bar{x}_1|^{1/2}\text{sign}(\bar{x}_1) + x_2 + \rho_1(x_1, t)\\ \frac{dx_2}{dt} &= -k_2\text{sign}(\bar{x}_1) + \rho_2(x_2, t)\end{aligned} \tag{2}$$

where x_i, $\bar{x}_i$, k_i, ρ_i, and sign() are state variables, error between estimated and actual state variables, sliding-mode coefficients, perturbation terms, and sign function, respectively.

The stable conditions of the above STA has been proved by Moreno *et al.* in [39] and [40]. According to [39] and [40], sliding mode coefficients of the above STA should satisfy (3) to stabilize the observer

$$k_1 > 2\delta_1,\ k_2 > k_1\frac{5\delta_1 k_1 + 4\delta_1^2}{2(k_1 - 2\delta_1)}. \tag{3}$$

And the perturbation terms should be globally bounded by

$$|\rho_1| \leqslant \delta_1|x_1|^{1/2},\ \rho_2 = 0 \tag{4}$$

where δ_1 is a positive constant.

B. Previous STA-SMO

Following [10], [16], the STA based stator current observers for PMSM sensorless control are constructed as follows:

$$\begin{aligned}\frac{d\hat{i}_\alpha}{dt} =& -\frac{R}{L}\hat{i}_\alpha + \frac{1}{L}u_\alpha + \frac{1}{L}k_1|\bar{i}_\alpha|^{1/2}\text{sign}(\bar{i}_\alpha)\\ &+ \frac{1}{L}\int k_2\text{sign}(\bar{i}_\alpha)dt\end{aligned} \tag{5a}$$

$$\begin{aligned}\frac{d\hat{i}_\beta}{dt} =& -\frac{R}{L}\hat{i}_\beta + \frac{1}{L}u_\beta + \frac{1}{L}k_1|\bar{i}_\beta|^{1/2}\text{sign}(\bar{i}_\beta)\\ &+ \frac{1}{L}\int k_2\text{sign}(\bar{i}_\beta)dt\end{aligned} \tag{5b}$$

where $\hat{}$ denotes estimated value.

When STA-SMO reaches to the equilibrium point, the estimated back-EMFs can be expressed as

$$\hat{e}_\alpha = -k_1|\bar{i}_\alpha|^{1/2}\text{sign}(\bar{i}_\alpha) - \int k_2\text{sign}(\bar{i}_\alpha)dt \tag{6a}$$

$$\hat{e}_\beta = -k_1|\bar{i}_\beta|^{1/2}\text{sign}(\bar{i}_\beta) - \int k_2\text{sign}(\bar{i}_\beta)dt. \tag{6b}$$

Basically, the STA-SMO for PMSM is derived based on $\alpha\beta$-axis voltage equations and the basic form of STA. Comparing with (1) and (2), it should be noticed that $-\frac{R}{L}i_\alpha + \frac{1}{L}u_\alpha$ and $-\frac{R}{L}i_\beta + \frac{1}{L}u_\beta$ are regarded as perturbation terms in STA. The back-EMFs in $\alpha\beta$-axis voltage equations are replaced by (6). Usually, k_2 is much larger than k_1. In (6), integration and large k_2 could reduce the chattering caused by sign function and k_1 could guarantee fast dynamic response of the observer. Hence, the estimated back-EMFs are affected by both k_1 and k_2.

The $\alpha\beta$-axis back-EMFs can be also expressed as [16]

$$e_\alpha = -\psi_f \omega \sin(\theta),\ e_\beta = \psi_f \omega \cos(\theta) \tag{7}$$

where ψ_f is the rotor flux linkage generated by permanent magnet.

Then, estimated rotor position can be calculated with the trigonometric function as

$$\hat{\theta} = \arctan\left(-\frac{\hat{e}_\alpha}{\hat{e}_\beta}\right). \tag{8}$$

And the estimated rotor speed can be calculated by differential of estimated rotor position

$$\hat{\omega} = \frac{d\hat{\theta}}{dt}. \tag{9}$$

C. Proposed Adaptive Algorithm for STA-SMO

From the above analysis, it can be seen that the stable conditions of STA-SMO is not explicit, different sets of k_1 and k_2 could lead to similar finite-time convergence of STA-SMO. In practice, it is difficult to decide the actual value of the sliding-mode coefficients. In [8], sliding-mode coefficients are set to $k_1 = 1.5\sqrt{f^+}$ and $k_2 = 1.1 f^+$, where f^+ is the upper bound of perturbation. However, large sliding-mode coefficients may lead to severe chattering and even instability in sensorless control system in low-speed range, where perturbation terms become smaller than that of high-speed range. On the contrary, small sliding-mode coefficients may cause instability in high-speed range, where conditions (4) cannot be satisfied. Therefore, online tuning the sliding-mode coefficients based on perturbation is necessary.

In this paper, the proposed adaptive algorithm for STA-SMO is given in (10). If sliding-mode coefficients k_1 and k_2 satisfy (10), the STA-SMO will be stable

$$k_1 = \sigma_1 \omega,\ k_2 = \sigma_2 \omega^2 \tag{10}$$

where σ_1 and σ_2 are adaptive coefficients.

The proof of the proposed adaptive algorithm is given below.

Proof: In real applications, the calculation frequency of speed calculation module is 1 kHz, while sampling frequency is 10 kHz. That is because rotor speed is calculated by position differential, chattering in rotor speed can be reduced by increasing the speed calculation period. It means that the estimated rotor speed keeps constant very 10 sampling periods. Therefore, estimated rotor speed or k_1, k_2 in (10) can be regarded as constant during stability analysis.

According to the stator current observer and the basic form of STA, perturbation term is expressed as

$$\rho_1 = -\frac{R}{L}\hat{i} + \frac{1}{L}u. \tag{11}$$

In most cases, voltages drop across stator resistance can be neglected. Thus, perturbation term ρ_1 can approximate to u/L and ρ_1 can be simplified as

$$\rho_1 \approx \frac{1}{L}u \approx \gamma_1 \omega \tag{12}$$

where $\gamma_1 = \frac{\psi_f}{L}$.

Then, the global limitation (4) can be rewritten as

$$|\rho_1| \approx |\gamma_1 \omega| \leqslant \delta_1 |\bar{i}|^{1/2}. \tag{13}$$

When the STA-SMO is stable, $|\bar{i}|^{1/2}$ is limited at a small range. Therefore, there must exist a large enough constant η_1 that satisfies the following inequality:

$$|\rho_1| \approx |\gamma_1 \omega| \leqslant \delta_1 \left|\bar{i}\right|^{1/2} = |\eta_1 \omega| \left|\bar{i}\right|^{1/2}\Big|. \tag{14}$$

In other words, δ_1 can be replaced by $\delta_1 = \eta_1 \omega$. Then, there must exists a large enough constant σ_1 that satisfies the first term of stable conditions ($k_1 = \sigma_1 \omega > 2\delta_1 = 2\eta_1 \omega$) easily.

Substituting $k_1 = \sigma_1 \omega$ and $\delta_1 = \eta_1 \omega$ into the second inequality of (3), the following inequality can be obtained:

$$k_2 > \sigma_1 \omega \frac{5\eta_1 \omega \cdot \sigma_1 \omega + 4\eta_1^2 \omega^2}{2(\sigma_1 \omega - 2\eta_1 \omega)} = \frac{\sigma_1(5\eta_1\sigma_1 + 4\eta_1^2)}{2(\sigma_1 - 2\eta_1)}\omega^2. \tag{15}$$

It is obvious that $\frac{\sigma_1(5\eta_1\sigma_1+4\eta_1^2)}{2(\sigma_1-2\eta_1)}$ can be seen as a constant. Assuming that $k_2 = \sigma_2 \omega^2$, there must exist a large enough constant σ_2 that satisfies (15) easily.

From the above analysis, it can be seen that the proposed adaptive algorithm $k_1 = \sigma_1 \omega$ and $k_2 = \sigma_2 \omega^2$ can satisfy the stable conditions (3). The stable conditions (3) have been proved by J. A. Moreno, *et. al.* in [39] and [40]. In other words, if the sliding-mode coefficients k_1 and k_2 satisfy the proposed adaptive algorithm, the STA-SMO presented in (5) will also be stable. At the same time, it should be noticed that the adaptive algorithm also make sure that the value of k_1, k_2 are limited under different speed and this is the main reason why the chattering of the proposed sensorless scheme is small in wide-speed range. ■

If $\rho_1 \approx \frac{1}{L}u \approx \gamma_1 \omega$ is not valid or estimated rotor speed is not accurate enough, their influence on position estimation can be ignored. This can be explained by two reasons. First, when the STA-SMO is stable, error between perturbation ρ_1 and $\gamma_1 \omega$ is limited in a small range. Similarly, error between real rotor speed and estimated rotor speed is also small when STA-SMO is stable. Second, although STA-SMO with constant sliding-mode coefficients k_1 and k_2 cannot work well in wide-speed range, it works well in medium-speed range. For example, in Fig. 2, the PMSM works well in a speed range of 1000 to 500 rpm under constant sliding-mode coefficients. In other words, similar k_1 and k_2 could lead to similar results. Therefore, errors caused by $\rho_1 \approx \frac{1}{L}u \approx \gamma_1 \omega$ approximation or speed estimation error can be neglected.

In practice, the initial sliding-mode coefficients are selected based on the existing stable conditions presented in (3). The details of obtaining σ_1 and σ_2 is explained as follows:

1) The PMSM is driven at a medium speed under open-loop control. In this paper, the speed command is set to $\omega_0 =$ 750 rpm (0.5 p.u.).
2) The initial sldiing-mode coefficients k_{10} and k_{20}, are selected based on the existing stable conditions (3). In particular, $k_{10} = 3$, $k_{20} = 19\,740$ is a valid choice in this paper.
3) Then, the adaptive coefficients can be calculated by

$$\sigma_1 = \frac{k_{10}}{\omega_0},\ \sigma_2 = \frac{k_{20}}{\omega_0^2}. \tag{16}$$

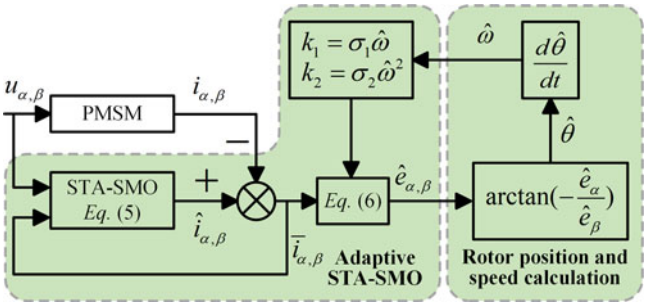

Fig. 1. Block diagram of the proposed adaptive STA-SMO.

The block diagram of adaptive STA-SMO is shown in Fig. 1. It should be noticed that estimated rotor speed instead of speed command is used for tuning k_1 and k_2 to improve the dynamic performance of the system. In this way, the sliding-mode coefficients can change with the rotor speed (perturbation) immediately and the sensorless control system will obtain stronger robustness against disturbance.

D. Discretized STA-SMO

The continuous STA-SMO must be discretized to implement on DSP. The discrete form of STA-SMO can be written as (the Euler scheme)

$$\hat{i}_x(n) = \frac{T}{L}u_x(n-1) + \left(1 - \frac{R}{L}T\right)\hat{i}_x(n-1) - \frac{T}{L}\hat{e}_x(n-1)$$

$$\hat{e}_x(n) = -k_1|\bar{i}_x(n-1)|^{1/2}\text{sign}(\bar{i}_x(n-1)) - z_x(n-1)$$

$$z_x(n) = z_x(n-1) + Tk_2\text{sign}(\bar{i}_x(n-1))$$

where x denotes $\alpha\beta$-axis, T is the sampling period, n is the index of discrete sampling instant, and $\bar{i}_x(n)$ is the error between estimated current and measured current ($\bar{i}_x(n) = \hat{i}_x(n) - i_x(n)$). If the sliding-mode coefficients k_1 and k_2 are selected based on the conditions presented in (10), the discrete STA-SMO will be stable and the corresponding experimental verification is given below.

E. Experimental Verification for the Proposed Adaptive STA-SMO

1) Wide-Speed Sensorless Operation: Experiments on a surface-mounted PMSM are conducted to verify the proposed adaptive algorithm. STA-SMO with large sliding-mode coefficients are presented in Fig. 2. The PMSM is started with encoder and switched to sensorless operation. The main parameters of the PMSM and control system are shown in Table I. In Fig. 2, since the PMSM cannot operate in low-speed range with large k_1 and k_2, the speed command is changed from 1000 to 200 rpm. It is obvious that the position estimation error becomes larger in low-speed range and finally the system becomes unstable at 280 rpm. That is because large k_1 and k_2 could bring chattering in low-speed range. On the contrary, STA-SMO with small sliding-mode coefficients are presented in Fig. 3. The speed command is changed from 200 to 1000 rpm. The system becomes unstable at about 630 rpm. That is because STA-SMO with small k_1 and k_2 may become unstable in high-speed range

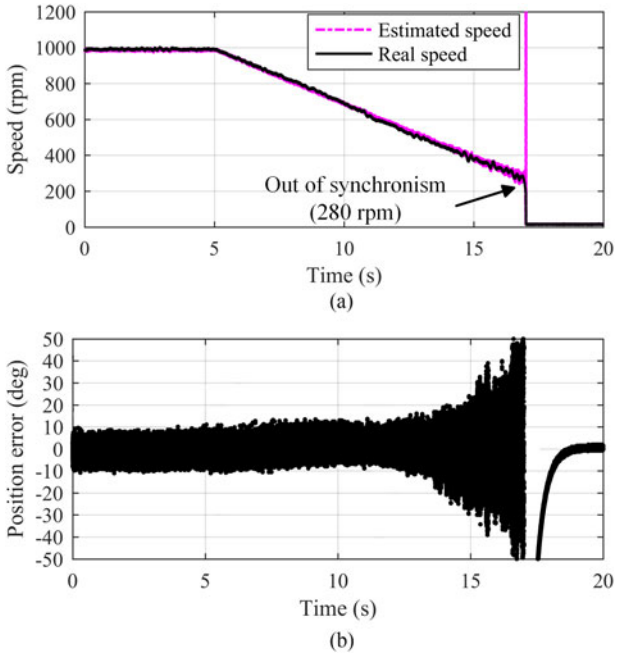

Fig. 2. Experimental results of STA-SMO with large sliding-mode coefficients ($k_1 = 4, k_2 = 35000$) under a 4 N·m load and speed command of 1000 to 200 rpm. (a) Rotor speed. (b) Position estimation error.

TABLE I
MAIN PARAMETERS OF PMSM[1] AND CONTROL SYSTEM

Items	Value
Stator resistance (Ω)	0.273
Rated current (A)	10
PM flux linkage (Wb)	0.1246
DC bus voltage (V)	200
Stator inductance (mH)	2.25
Rated speed (rpm)	1500
Pole pairs	5
Rated torque (N·m)	9.6
Rated power (kW)	1.5
Dead-time (μs)	2
Turn-on delay[2] (μs)	0.3–2
Turn-off delay[2] (μs)	1.2–2.8
Saturation voltage[2] (V)	1.7–2.4
Diode forward voltage[2] (V)	2.3–3.3
Switching frequency (kHz)	10
Sampling frequency (kHz)	10

[1] Huada LDD-130ST-M0961530LMDD,
[2] Mitsubishi data sheet (PM75RL1A120).

where perturbation is too large to satisfy (4). Experimental results presented in Figs. 2 and 3 illustrate that the performance of STA-SMO with constant sliding-mode coefficients is poor and online tuning the sliding-mode coefficients is necessary.

After applying the proposed adaptive algorithm, the sensorless control system works well as shown in Fig. 4. The speed command is changed from 1000 to 200 rpm. The position estimation error is lower than that with constant sliding-mode coefficients in wide-speed range. Thus, the effectiveness of the proposed adaptive STA-SMO for wide-speed sensorless operation could be verified.

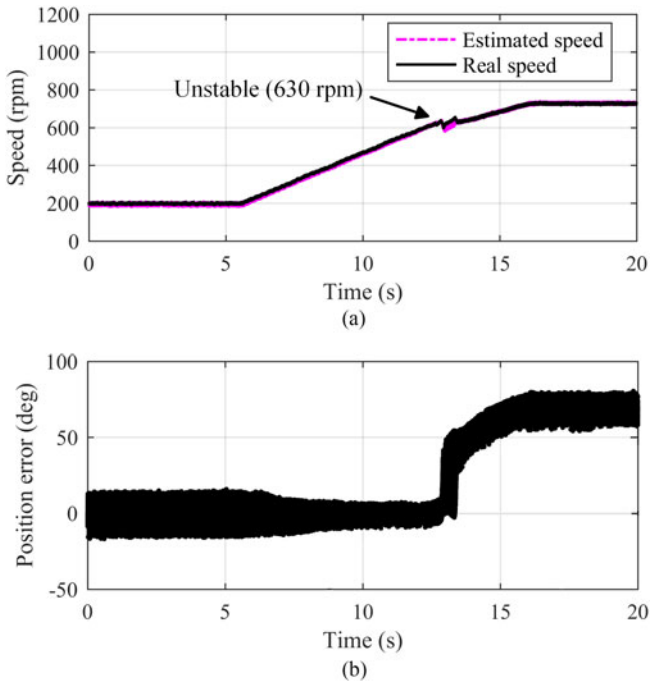

Fig. 3. Experimental results of STA-SMO with small sliding-mode coefficients ($k_1 = 2, k_2 = 8750$) under a 4 N·m load and speed command of 200 to 1000 rpm. (a) Rotor speed. (b) Position estimation error.

2) Dynamic Performance: The dynamic performance of the proposed adaptive STA-SMO is investigated in this section. The experimental results are shown in Fig. 5. In order to investigate the dynamic performance of the system, a 9.6 N·m step load is enabled and disabled successively as shown in Fig. 5(a) and (b). It can be seen that both of the position estimation errors remain almost the same after a 9.6 N·m step load is enabled. It can be explained that the velocity drop is small and chattering in position estimation error can be neglected. However, compared to adaptive STA-SMO, the position estimation error of STA-SMO with constant sliding-mode coefficients becomes much larger when step load is disabled. That is because overshoot in rotor speed makes perturbation become larger, which means (4) is not satisfied. After applying the adaptive algorithm in Fig. 5(f), the sliding-mode coefficients change with the estimated rotor speed and the adaptive STA-SMO works well under dynamic situations. Therefore, it can be concluded that the dynamic performance and robustness against disturbance of STA-SMO has been improved greatly with the proposed adaptive algorithm.

III. VSI Nonlinearity Compensation

VSI nonlinearity is mainly caused by dead-time ($T_{\rm d}$), turn-on delay ($T_{\rm on}$), turn-off delay ($T_{\rm off}$), etc. In medium or high speed range, VSI nonlinearity can be ignored, because the duty ratio of switches is high. However, VSI nonlinearity may become dominant in low-speed range and has a great influence on sensorless operation. The influence of VSI nonlinearity on dq-axis reference voltages at 150 rpm and rated load is given in Fig. 6. Main parameters of the machine and control system are given in Table I. A 2 μs dead-time is enabled at 0.25 s. It is obvious

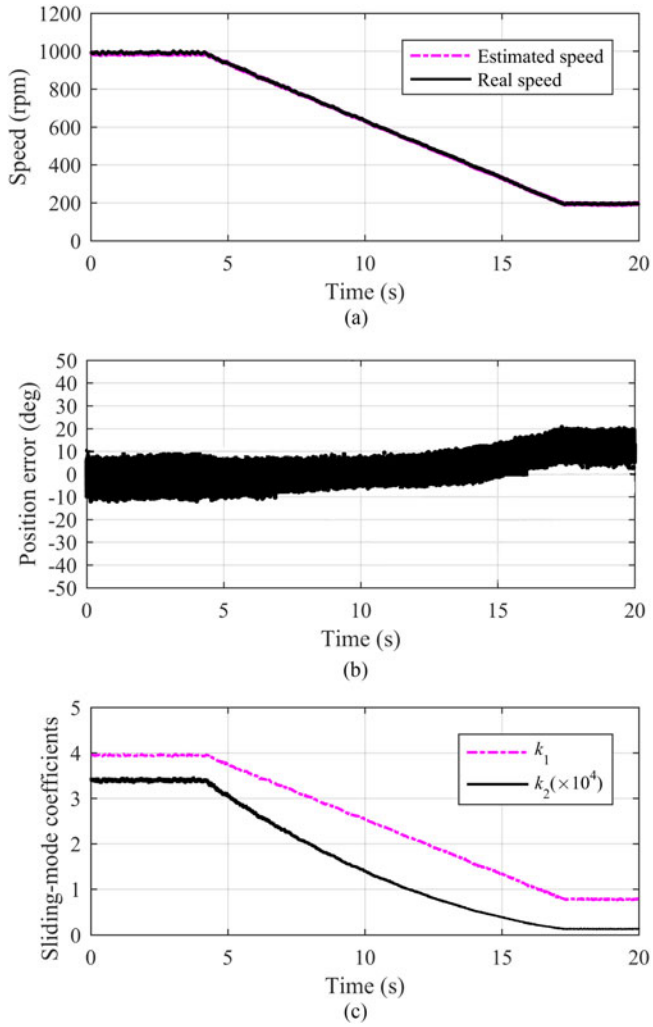

Fig. 4. Experimental results of adaptive STA-SMO ($\sigma_1 = 0.00764$, $\sigma_2 = 0.128$) under a 4 N·m load and speed command of 1000 to 200 rpm. (a) Rotor speed. (b) Position estimation error. (c) Sliding-mode coefficients.

that VSI nonlinearity has a great influence on dq-axis reference voltages. Since reference voltages are used for position estimation, mismatch in voltages will cause position estimation error. The impact of VSI nonlinearity on position estimation can be also seen at Fig. 4(b). The position estimation error becomes larger in low-speed range, which is mainly caused by VSI nonlinearity. Therefore, VSI nonlinearity must be compensated to improve the position estimation accuracy.

A. VSI Nonlinearity Analysis

If VSI nonlinearity is taken into consideration, the actual machine model in rotating reference frame can be written as

$$\begin{aligned} L_d \frac{di_d}{dt} &= -Ri_d + L_q \omega i_q + u_d^* + V_{\rm dead} Dd \\ L_q \frac{di_q}{dt} &= -Ri_q - L_d \omega i_d - \psi_m \omega + u_q^* + V_{\rm dead} Dq \end{aligned} \tag{17}$$

where $V_{\rm dead}$ is the magnitude of the distorted voltages and Dd, Dq are coefficients decided by direction of phase currents and electrical position θ. $V_{\rm dead}$, Dd and Dq can be expressed as

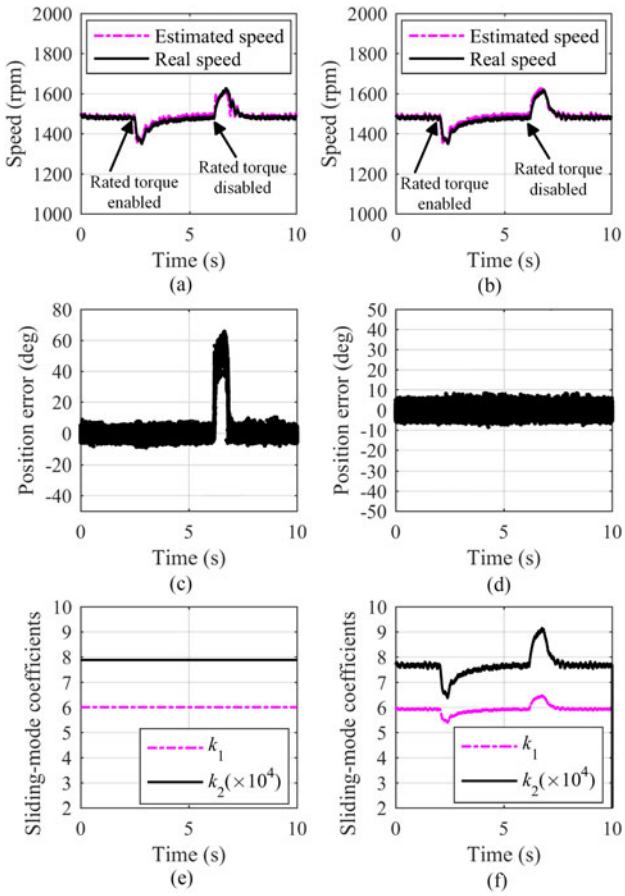

Fig. 5. Dynamic performance of STA-SMO with constant sliding-mode coefficients and the proposed adaptive algorithm at a speed command of 1500 rpm. (a), (c), (e) With constant sliding-mode coefficients ($k_1 = 6$, $k_2 = 78750$). (b), (d), (f) With the proposed adaptive algorithm ($\sigma_1 = 0.00764$, $\sigma_2 = 0.128$).

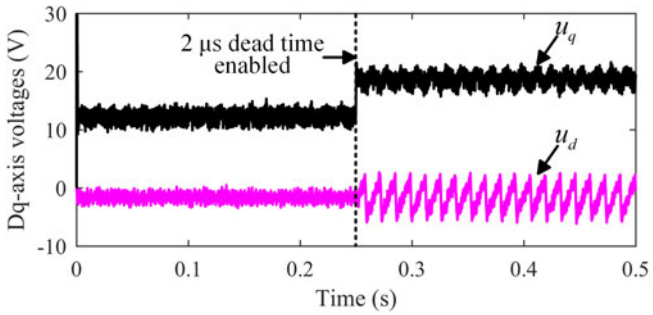

Fig. 6. Simulation results of VSI nonlinearity's effect on dq-axis voltages.

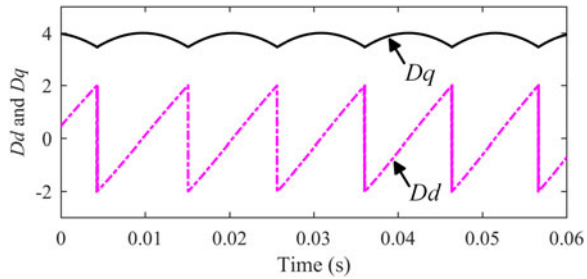

Fig. 7. Simulation waveforms of Dd and Dq under $i_d = 0$ control and speed command of 200 rpm.

follows [29], [41]:

$$V_{\text{dead}} = \frac{T_{\text{dead}} + T_{\text{on}} - T_{\text{off}}}{T_s} u_{\text{dc}} \tag{18a}$$

$$\begin{bmatrix} Dd \\ Dq \end{bmatrix} = 2 \begin{bmatrix} \cos(\theta) & \cos\left(\theta - \frac{2\pi}{3}\right) & \cos\left(\theta + \frac{2\pi}{3}\right) \\ -\sin(\theta) & -\sin\left(\theta - \frac{2\pi}{3}\right) & -\sin\left(\theta + \frac{2\pi}{3}\right) \end{bmatrix} \times \begin{bmatrix} \text{sign}(i_a) \\ \text{sign}(i_b) \\ \text{sign}(i_c) \end{bmatrix} \tag{18b}$$

$$\text{sign}(x) = \begin{cases} 1, & x \geqslant 0 \\ -1, & x < 0. \end{cases} \tag{18c}$$

The magnitude of the distorted voltage V_{dead} is a function of dead-time, turn-on delay, turn-off delay, and dc bus voltage. Dead-time and dc bus voltage can be obtained easily, while the turn-on delay and turn-off delay are dependent on operation states such as dc bus voltage and phase currents. Therefore, compensating VSI nonlinearity by off-line measuring the turn-on/off delay is difficult. In this paper, V_{dead} is calculated online to compensate the VSI nonlinearity.

The simulated waveforms of Dd and Dq under $i_d = 0$ control and speed command of 200 rpm is shown in Fig. 7. It is obvious that the mean value of Dd is zero, while it composes a large sixth harmonic component. On the contrary, Dq mainly consists a dc component and a small sixth harmonic component.

B. Online VSI Nonlinearity Compensation

In this paper, a simple and effective VSI nonlinearity compensation method is proposed, which is machine parameter-independent and works well under $i_d = 0$ control.

It has been proved in [41] that the high frequency components of d-axis reference voltage under $i_d = 0$ control is approximately equal to the d-axis distorted voltage. The proposed VSI nonlinearity compensation algorithm is presented in Fig. 8. In this paper, V_{dead} is extracted using LPFs as shown in Fig. 9. In Fig. 9, u_{d2}^* is the d-axis reference voltage used to calculate the duty ratio of switches. Its actual position is shown in Fig. 8. $u_{d2\_hf}^*$ is the high frequency components of u_{d2}^*. Since $u_{d2\_hf}^* \approx V_{\text{dead}} Dd$, V_{dead} can be calculated by $V_{\text{dead}} \approx u_{d2\_hf}^* / Dd$. However, since there are zero crossing points in Dd, a limitation on Dd is necessary to prevent overflow. Thus, Dd is replaced by $Dd^{'}$ and the expression of $Dd^{'}$ is shown as follows:

$$Dd^{'} = \begin{cases} Dd, & 0.2 \leqslant |Dd| \leqslant 2 \\ 0.2, & 0 \leqslant Dd < 0.2 \\ -0.2, & -0.2 < Dd < 0 \end{cases} \tag{19}$$

where the threshold 0.2 is tuned by experiments. Since the threshold is small, its influence on VSI compensation can be neglected.

The second LPF shown in Fig. 9 is used to smoothen the V_{dead}. In this paper, cut off frequency of both two LPFs is set to 5 Hz. It should be noticed that V_{dead} cannot be extracted using q-axis

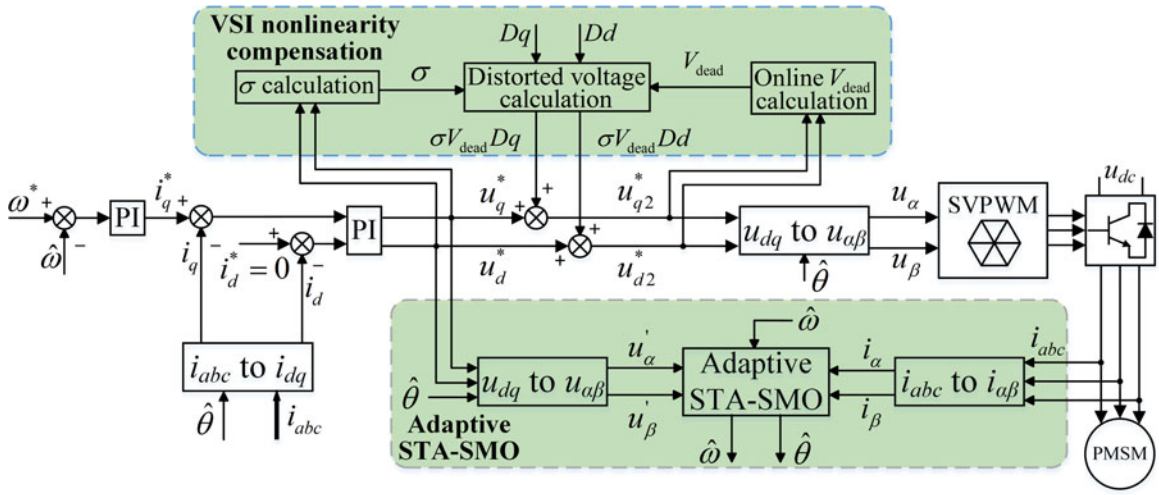

Fig. 8. Whole sensorless control system diagram with the proposed adaptive STA-SMO and VSI nonlinearity compensation.

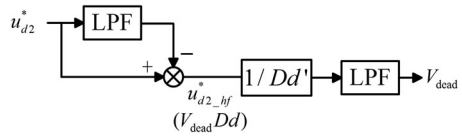

Fig. 9. V_{dead} calculation.

voltage, because q-axis voltage consist both dc component and high frequency components. Therefore, only d-axis voltage is used for V_{dead} calculation.

In practice, if distorted voltages are injected into reference voltages directly, VSI nonlinearity cannot be well compensated. Because the nonlinearity of the control system may deteriorate the compensation and, hence, online tuning the compensated voltages is necessary [41].

In this research, VSI nonlinearity is compensated by minimizing $V_{\text{dead}}^{'}$. It should be noticed that $V_{\text{dead}}^{'}$ is different from V_{dead}. $V_{\text{dead}}^{'}$ is obtained using the same method shown in Fig. 9, but the input signal is u_d^*, where u_d^* is the reference voltage value generated by current PI regulator and its actual position is shown in Fig. 8.

The flow chart of $V_{\text{dead}}^{'}$ minimization is shown in Fig. 10. In Fig. 10, V_{thr} is the threshold voltage of $V_{\text{dead}}^{'}$, σ is the gain factor, and λ is the tuning factor. It should be noticed that λ can control the compensation speed and large λ may cause abrupt change in control system. Therefore, λ is initialized to 0.0001 in this paper. The working process of Fig. 10 is explained as follows:

1) Initialization: $V_{\text{thr}} = 0.1$ V, $\sigma = 0$, $\lambda = 0.0001$.
2) If $|V_{\text{dead}}^{'}| < V_{\text{thr}}$, it means that the VSI nonlinearity is well compensated and there is no need to change σ.
3) If $V_{\text{dead}}^{'} < -V_{thr}$, it means that the VSI nonlinearity is over compensated and σ needs to be smaller.
4) If $V_{\text{dead}}^{'} > V_{\text{thr}}$, it means that the VSI nonlinearity is not well compensated and σ needs to be larger.
5) Inject $\sigma V_{\text{dead}} Dd$ and $\sigma V_{\text{dead}} Dq$ into dq-axis reference voltages, respectively.
6) Go back to step 2.

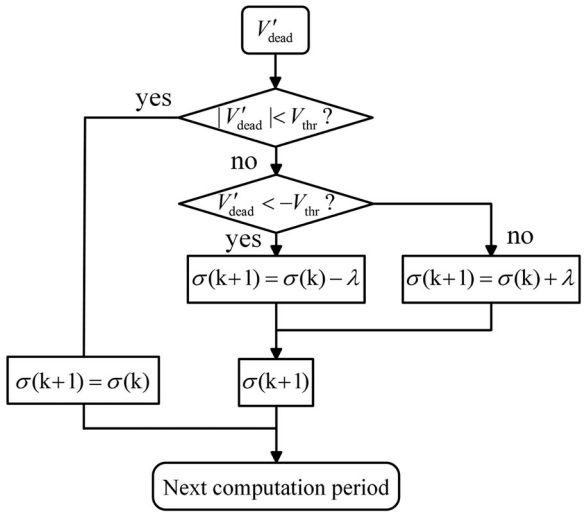

Fig. 10. Flow chart of $V_{\text{dead}}^{'}$ minimization.

C. Experimental Verification for the Proposed VSI Nonlinearity Compensation

In order to verify the effectiveness of the proposed VSI nonlinearity compensation method, the control system is operated with an encoder, which means the adaptive STA-SMO in Fig. 8 is disabled and rotor position and speed are obtained by encoder. $i_d = 0$ field oriented control is employed in this paper. The main parameters of PMSM and control system are detailed in Table I. Fig. 11 shows the experimental results with and without the proposed compensation strategy. The PMSM operates with a 10 N·m load at 200 rpm. Comparing Fig. 11(a) with Figs. 6 and 7, it is evident that the measured dq-axis voltages agree well with the simulated waveforms, which include sixth harmonic components. Besides, there are fifth and seventh harmonic components in phase current as shown in Fig. 11(e) and (g). After compensation, sixth harmonic components in dq-axis currents and voltages are eliminated. Furthermore, q-axis voltage reduces greatly and the mean value of d-axis voltage remains almost the same,

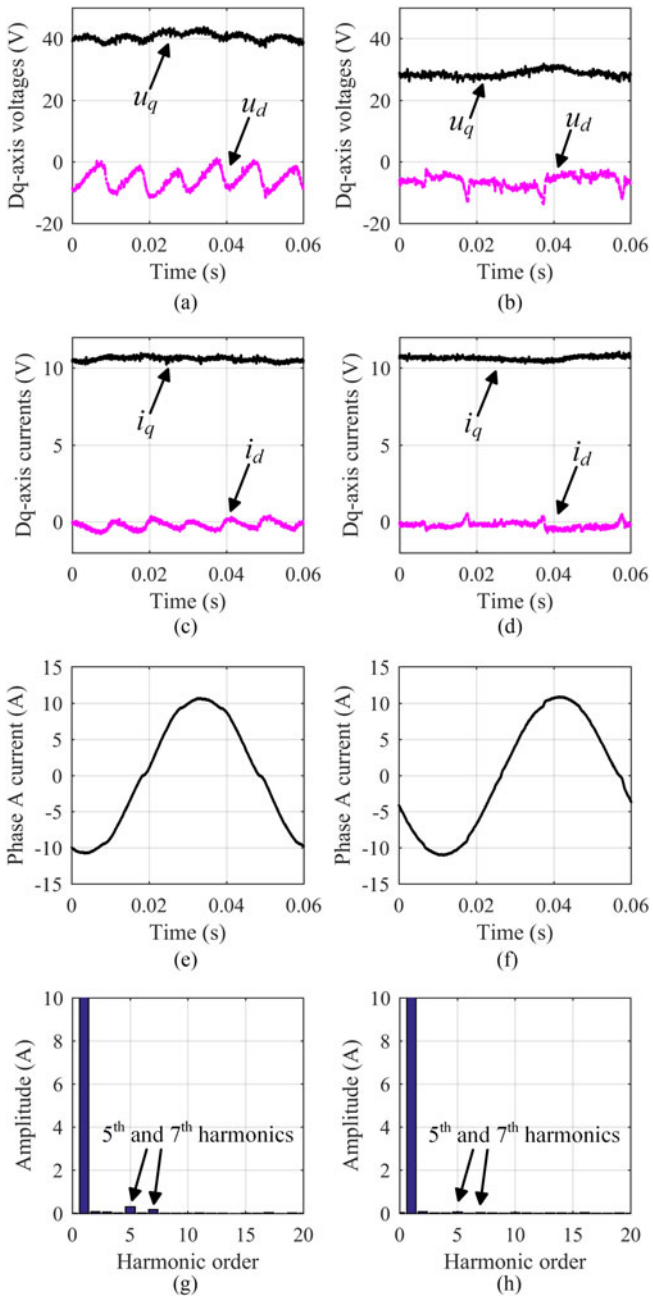

Fig. 11. Experimental verification for the proposed VSI nonlinearity compensation method. (a), (c), (e), (g) Without compensation, (b), (d), (f), (h) With the proposed compensation.

which makes the phase current more sinusoidal. The fifth and seventh harmonic components in phase current can be neglected as shown in Fig. 11(f) and (h). These improvements help to establish a more accurate PMSM model and improve the position estimation accuracy. Besides, the proposed VSI nonlinearity compensation method is machine parameter-independent, which means that the proposed VSI nonlinearity compensation method is robust against machine parameter variation.

IV. Comprehensive Experimental Results

The whole sensorless control system diagram with the proposed adaptive STA-SMO and online VSI nonlinearity

Fig. 12. Experimental setup.

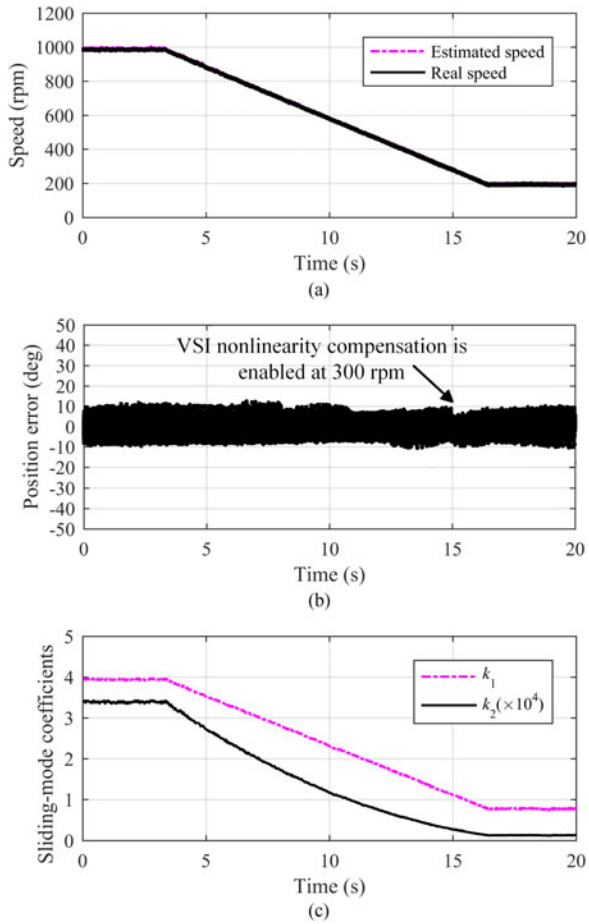

Fig. 13. Experimental results of adaptive STA-SMO ($\sigma_1 = 0.00764$, $\sigma_2 = 0.128$) and VSI nonlinearity compensation under a 4 N·m load and speed command of 1000 rpm to 200 rpm. (a) Rotor speed. (b) Position estimation error. (c) Sliding-mode coefficients.

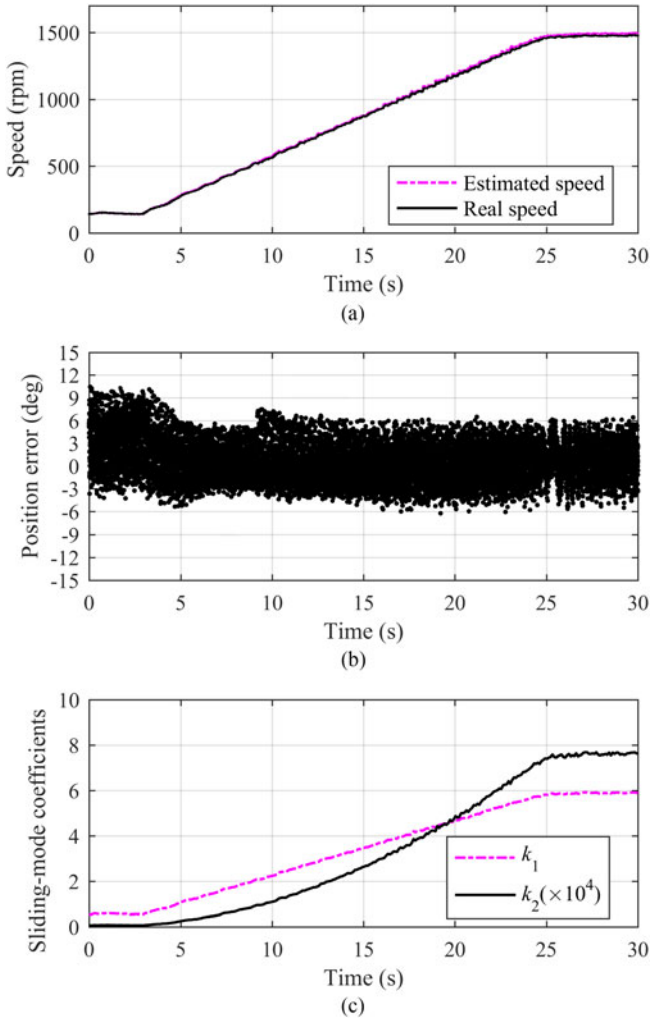

Fig. 14. Experimental results of the proposed adaptive STA-SMO and VSI nonlinearity compensation under rated load and speed command of 150 to 1500 rpm. (a) Rotor speed. (b) Position estimation error. (c) Sliding-mode coefficients.

compensation is shown in Fig. 8. Details of the VSI nonlinearity compensation and adaptive STA-SMO have been introduced in Sections II and III. To combine the adaptive STA-SMO with the VSI nonlinearity compensation, the dq-axis reference voltages u_d^* and u_q^* are used for position estimation. In other words, $u_\alpha^{'}$ and $u_\beta^{'}$, instead of u_α and u_β, are used for sensorless control. Besides, both of the reference voltages before and after compensation are used for online VSI nonlinearity compensation. Main parameters of the whole system are given in Table I. The experimental setup is shown in Fig. 12. The surface-mounted PMSM is controlled by DSP TMS320F28335 and fed by a Mitsubishi PM75RL1A120 intelligent power module.

The experimental results of the proposed adaptive STA-SMO with VSI nonlinearity compensation are shown in Fig. 13. The PMSM is operated under a 4 N·m load and speed command of 1000 to 200 rpm. Since the influence of VSI nonlinearity can be ignored in high-speed range, the proposed VSI nonlinearity compensation is activated only in low-speed range. Compared to Fig. 4, it is obvious that the position estimation error is reduced greatly after VSI nonlinearity is compensated. That is because

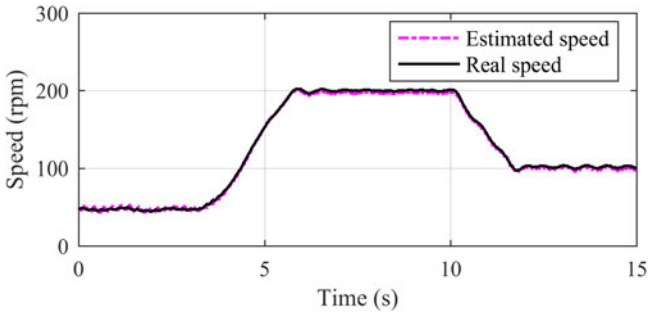

Fig. 15. Low speed operation with the proposed sensorless technique.

the reference voltage used for position estimation is more accurate after compensation. Thus, the effectiveness of the adaptive STA-SMO with online VSI nonlinearity compensation could be verified.

The proposed sensorless technique is also tested under rated load and a speed command of 150 to 1500 rpm. The experimental results are presented in Fig. 14. The VSI nonlinearity compensation is disabled when the speed is higher than 500 rpm. It can be seen that, the position estimation error is restricted in a small region in either low-speed range or high-speed range. It proves that the proposed adaptive STA-SMO with online VSI nonlinearity compensation could operate in wider speed range. Further, the proposed online VSI nonlinearity compensation could reduce the position estimation error in low-speed range.

Finally, the proposed sensorless control technique is tested in low speed range. Fig. 15 shows the acceleration/deceleration process of the PMSM, where the speed command is changed from 50 rpm to 200 rpm and then to 100 rpm. It can be seen that the PMSM works well in low-speed range. The experimental results have verified the effectiveness of the proposed sensorless technique.

V. Conclusion

In this paper, a sensorless control technique based on an adaptive STA-SMO and online VSI nonlinearity compensation is proposed. The proposed adaptive algorithm is obtained based on the existing stable conditions to guarantee the stability of STA-SMO. At the same time, a machine parameter-independent, simple and effective method is used to online compensate the VSI nonlinearity. Thus, an adaptive STA-SMO with accurate PMSM model is obtained. Experimental results show that the proposed adaptive algorithm could reduce the position estimation error under wide-speed range sensorless operation. Especially, position estimation error in low-speed range is reduced greatly by compensating the VSI nonlinearity. Furthermore, the PMSM works well in dynamic situation due to the adaptive algorithm. Compared to the existing STA-SMO based sensorless techniques, the proposed adaptive algorithm and VSI nonlinearity compensation method are simple, so the proposed technique is easy to be implemented in the real system. However, since the sensorless control technique is designed based on machine model, its observability is lost at ultra-low speed and zero speed. Thus, ultra-low speed and zero speed sensorless operation still needs further investigation.

REFERENCES

[1] M.-H. Park and H.-H. Lee, "Sensorless vector control of permanent magnet synchronous motor using adaptive identification," in *Proc. IEEE Annu. Conf. Ind. Electron. Soc.*, Nov. 1989, vol. 1, pp. 209–214.

[2] D. Kim, Y. C. Kwon, S. K. Sul, J. H. Kim, and R. S. Yu, "Suppression of injection voltage disturbance for high-frequency square-wave injection sensorless drive with regulation of induced high-frequency current ripple," *IEEE Trans. Ind. Appl.*, vol. 52, no. 1, pp. 302–312, Jan. 2016.

[3] R. Ni, D. Xu, F. Blaabjerg, K. Lu, G. Wang, and G. Zhang, "Square-wave voltage injection algorithm for PMSM position sensorless control with high robustness to voltage errors," *IEEE Trans. Power Electron.*, vol. 32, no. 7, pp. 5425–5437, Jul. 2017.

[4] T. C. Lin and Z. Q. Zhu, "Sensorless operation capability of surface-mounted permanent-magnet machine based on high-frequency signal injection methods," *IEEE Trans. Ind. Appl.*, vol. 51, no. 3, pp. 2161–2171, May 2015.

[5] Y. Shi, K. Sun, L. Huang, and Y. Li, "Online identification of permanent magnet flux based on extended kalman filter for IPMSM drive with position sensorless control," *IEEE Trans. Ind. Electron.*, vol. 59, no. 11, pp. 4169–4178, Nov. 2012.

[6] N. K. Quang, N. T. Hieu, and Q. P. Ha, "Fpga-based sensorless PMSM speed control using reduced-order extended kalman filters," *IEEE Trans. Ind. Electron.*, vol. 61, no. 12, pp. 6574–6582, Dec. 2014.

[7] L. Zhao, J. Huang, H. Liu, B. Li, and W. Kong, "Second-order sliding-mode observer with online parameter identification for sensorless induction motor drives," *IEEE Trans. Ind. Electron.*, vol. 61, no. 10, pp. 5280–5289, Oct. 2014.

[8] V. C. Ilioudis, "Chattering reduction applied in PMSM sensorless control using second order sliding mode observer," in *Proc. 9th Int. Conf. Compat. Power Electron.*, Jun. 2015, pp. 240–245.

[9] M. Ezzat, J. de Leon, N. Gonzalez, and A. Glumineau, "Observer-controller scheme using high order sliding mode techniques for sensorless speed control of permanent magnet synchronous motor," in *Proc. 49th IEEE Conf. Decis. Control*, Dec. 2010, pp. 4012–4017.

[10] D. Liang, J. Li, and R. Qu, "Sensorless control of permanent magnet synchronous machine based on second-order sliding-mode observer with online resistance estimation," *IEEE Trans. Ind. Appl.*, vol. 53, no. 4, pp. 3672–3682, Jul. 2017.

[11] C. B. Regaya, F. Farhani, A. Zaafouri, and A. Chaari, "An adaptive sliding-mode speed observer for induction motor under backstepping control," *ICIC Express Lett.*, vol. 11, no. 4, pp. 763–772, 2017.

[12] Y. Park and S. K. Sul, "Sensorless control method for pmsm based on frequency-adaptive disturbance observer," *IEEE Trans. Emerg. Sel. Topics Power Electron.*, vol. 2, no. 2, pp. 143–151, Jun. 2014.

[13] T. Bernardes, V. F. Montagner, H. A. Grndling, and H. Pinheiro, "Discrete-time sliding mode observer for sensorless vector control of permanent magnet synchronous machine," *IEEE Trans. Ind. Electron.*, vol. 61, no. 4, pp. 1679–1691, Apr. 2014.

[14] G. Wang, L. Yang, G. Zhang, X. Zhang, and D. Xu, "Comparative investigation of pseudorandom high-frequency signal injection schemes for sensorless ipmsm drives," *IEEE Trans. Power Electron.*, vol. 32, no. 3, pp. 2123–2132, Mar. 2017.

[15] V. I. Utkin, J. Guldner, and J. Shi, *Sliding Mode Control in Electro-Mechanical Systems*. Boca Raton, FL, USA: CRC Press;, 2009.

[16] S. D. Gennaro, J. Rivera, and B. Castillo-Toledo, "Super-twisting sensorless control of permanent magnet synchronous motors," in *Proc. 49th IEEE Conf. Decis. Control*, Dec. 2010, pp. 4018–4023.

[17] J. R. Domnguez, A. Navarrete, M. A. Meza, A. G. Loukianov, and J. Caedo, "Digital sliding-mode sensorless control for surface-mounted pmsm," *IEEE Trans. Ind. Informat.*, vol. 10, no. 1, pp. 137–151, Feb. 2014.

[18] D. Zaltni and M. Ghanes, "Observability analysis and improved zero speed position observer design of synchronous motor with experimental results," *Asian J. Control*, vol. 15, no. 4, pp. 957–970, 2013.

[19] S. D. Gennaro, J. R. Domnguez, and M. A. Meza, "Sensorless high order sliding mode control of induction motors with core loss," *IEEE Trans. Ind. Electron.*, vol. 61, no. 6, pp. 2678–2689, Jun. 2014.

[20] M. Ezzat, J. de Leon, and A. Glumineau, "Sensorless speed control of PMSM via adaptive interconnected observer," *Int. J. Control*, vol. 84, no. 11, pp. 1926–1943, 2011.

[21] C. B. Regaya, F. Farhani, A. Zaafouri, and A. Chaari, "A novel adaptive control method for induction motor based on backstepping approach using dspace ds 1104 control board," *Mech. Syst. Signal Process.*, vol. 100, pp. 466–481, 2018.

[22] S. Lin and W. Zhang, "An adaptive sliding-mode observer with a tangent function-based PLL structure for position sensorless PMSM drives," *J. Elect. Power Energy Syst.*, vol. 88, pp. 63–74, 2017.

[23] R. Jon, Z. Wang, C. Luo, and M. Jong, "Adaptive robust speed control based on recurrent elman neural network for sensorless PMSM servo drives," *Neurocomput.*, vol. 227, pp. 131–141, 2017.

[24] A. Zaafouri, C. B. Regaya, H. B. Azza, and A. Chari, "Dsp-based adaptive backstepping using the tracking errors for high-performance sensorless speed control of induction motor drive," *ISA Trans*, vol. 60, pp. 333–347, 2016.

[25] F. Farhani, C. B. Regaya, A. Zaafouri, and A. Chaari, "Real time pi-backstepping induction machine drive with efficiency optimization," *ISA Trans*, vol. 70, pp. 348–356, 2017.

[26] C. B. Regaya, A. Zaafouri, and A. Chaari, "Speed sensorless indirect field-oriented of induction motor using two type of adaptive observer," in *Proc. 2013 Int. Conf. Elect. Eng. Softw. Appl.*, Mar. 2013, pp. 1–5.

[27] C. B. Regaya, F. Farhani, A. Zaafouri, and A. Chaari, "High-performance control of im using mras-fuzzy logic observer," *Int. J. Tomograph. Simul.*, vol. 30, no. 2, pp. 40–52, 2017.

[28] C. B. Regaya, F. Farhani, A. Zaafouri, and A. Chaari, "Comparison between two methods for adjusting the rotor resistance," *Int. Rev. Model. Simul.*, vol. 5, pp. 938–945, 2012.

[29] H.-S. Kim, K.-H. Kim, and M.-J. Youn, "On-line dead-time compensation method based on time delay control," *IEEE Trans. Control Syst. Technol.*, vol. 11, no. 2, pp. 279–285, Mar. 2003.

[30] H.-S. Kim, H.-T. Moon, and M.-J. Youn, "On-line dead-time compensation method using disturbance observer," *IEEE Trans. Power Electron.*, vol. 18, no. 6, pp. 1336–1345, Nov. 2003.

[31] H. W. Kim, H. S. Kim, M. J. Youn, and K. Y. Cho, "Online observation and compensation of voltage distortion in PWM VSI for PMSM," *IEE Proc. Elect. Power Appl.*, vol. 151, no. 5, pp. 534–542, Sep. 2004.

[32] S. H. Hwang and J. M. Kim, "Dead time compensation method for voltage-fed PWM inverter," *IEEE Trans. Energy Convers.*, vol. 25, no. 1, pp. 1–10, Mar. 2010.

[33] S. Y. Kim, W. Lee, M. S. Rho, and S. Y. Park, "Effective dead-time compensation using a simple vectorial disturbance estimator in pmsm drives," *IEEE Trans. Ind. Electron.*, vol. 57, no. 5, pp. 1609–1614, May 2010.

[34] Y. Park and S. K. Sul, "A novel method utilizing trapezoidal voltage to compensate for inverter nonlinearity," *IEEE Trans. Power Electron.*, vol. 27, no. 12, pp. 4837–4846, Dec. 2012.

[35] K. Liu, Z. Q. Zhu, Q. Zhang, and J. Zhang, "Influence of nonideal voltage measurement on parameter estimation in permanent-magnet synchronous machines," *IEEE Trans. Ind. Electron.*, vol. 59, no. 6, pp. 2438–2447, Jun. 2012.

[36] A. Levant, "Sliding order and sliding accuracy in sliding mode control," *Int. J. Control*, vol. 58, no. 6, pp. 1247–1263, 1993.

[37] P. R. Kumar, A. K. Behera, and B. Bandyopadhyay, "Robust finite-time tracking of stewart platform: A super-twisting like observer-based forward kinematics solution," *IEEE Trans. Ind. Electron.*, vol. 64, no. 5, pp. 3776–3785, May 2017.

[38] J. R. Dominguez, C. Mora-Soto, S. Ortega-Cisneros, J. J. R. Panduro, and A. G. Loukianov, "Copper and core loss minimization for induction motors using high-order sliding-mode control," *IEEE Trans. Ind. Electron.*, vol. 59, no. 7, pp. 2877–2889, Jul. 2012.

[39] J. A. Moreno and M. Osorio, "A lyapunov approach to second-order sliding mode controllers and observers," in *Proc. 47th IEEE Conf. Decis. Control*, Dec. 2008, pp. 2856–2861.

[40] J. A. Moreno and M. Osorio, "Strict lyapunov functions for the super-twisting algorithm," *IEEE Trans. Autom. Control*, vol. 57, no. 4, pp. 1035–1040, Apr. 2012.

[41] K. Liu and Z. Q. Zhu, "Online estimation of the rotor flux linkage and voltage-source inverter nonlinearity in permanent magnet synchronous machine drives," *IEEE Trans. Power Electron.*, vol. 29, no. 1, pp. 418–427, Jan. 2014.

Donglai Liang (S'15) was born in Guangdong, China in 1990. He received the B.E.E. degree in electrical engineering from the Huazhong University of Science and Technology, Wuhan, China, in 2013. He is currently working toward the Ph.D. degree in electrical engineering at the School of Electronic and Electrical Engineering, Huazhong University of Science and Technology, Wuhan, China.

His research interests include PM machine design and control.

Jian Li (M'10) received the B.E.E degree in electrical engineering from the Dalian University of Technology, Dalian, China, in 2005, and the M.S.E.E and Ph.D. degrees in electrical engineering from Dong-A University, Busan, Korea, in 2007 and 2011, respectively.

He is currently an Associate Research Professor with the School of Electrical and Electronic Engineering, Huazhong University of Science and Technology, Wuhan, China. His research interests include design and control of PM machines and reluctance machines.

Ronghai Qu (S'01–M'02–SM'05–F'17) was born in China. He received the B.E.E. and M.S.E.E. degrees in electrical engineering from Tsinghua University, Beijing, China, in 1993 and 1996, respectively, and the Ph.D. degree in electrical engineering from the University of Wisconsin-Madison, Madison, WI, USA, in 2002.

In 1998, he was a Research Assistant with the Wisconsin Electric Machines and Power Electronics Consortiums. He was a Senior Electrical Engineer with Northland, a Scott Fetzer Company, in 2002. Since 2003, he has been with the Electrical Machines and Drives Laboratory, General Electric (GE) Global Research Center, Niskayuna, NY, USA, as a Senior Electrical Engineer. He has authored or coauthored more than 120 published technical papers and is the holder of more than 50 patents/patent applications. Since 2010, he has been a Professor with the Huazhong University of Science and Technology, Wuhan, China.

Dr. Qu is a Full Member of Sigma Xi. Since 2003, he has been the recipient of several awards from the GE Global Research Center, including the Technical Achievement and Management Awards. He is also the recipient of the 2003 and 2005 Best Paper Awards, third prize, from the Electric Machines Committee of the IEEE Industry Applications Society at the 2002 and 2004 IAS Annual Meetings, respectively.

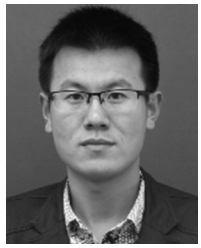

Wubin Kong (M'15) was born in Zhejiang, China, in 1986. He received the B.S. and Ph.D. degrees in power electronics and motor drives from Zhejiang University, Hangzhou, China in 2009 and 2014, respectively.

His research interests include high-power multiphase motor drives and fault tolerant control motor drives applied in EV. From 2015, he has been a Lecturer with the Huazhong University of Science and Technology, Wuhan, China.